In Situ Time-Dependent Signatures of Light Scattered from Solutions undergoing Polymerization Reactions

Alina M. Alb, Emmanuel Mignard,† Michael F. Drenski, and Wayne F. Reed*

Department of Physics, Tulane University, New Orleans, Louisiana 70118

Received December 4, 2003; Revised Manuscript Received January 14, 2004

ABSTRACT: Time-dependent static light scattering (TDSLS) signatures were used to characterize polymerization reactions in situ. The relationship between these signatures and intra- and interparticle characteristics of the growing polymer population, as the solution passes from the dilute to semidilute regime, is sought theoretically, and measured experimentally. As much information as possible is determined concerning polymer mass and polymerization kinetics. At the outset of the reactions the weight-average molecular mass M_w dominates the scattered intensity, but gives way to second and third virial coefficient (A_2, A_3) effects as polymer concentration increases. Since polymer mass, A_2 and A_3 are interrelated, it is possible to introduce plausible conversion kinetics to predict a variety of TDSLS signatures. These are calculated for free radical and controlled radical polymerization and compared to experimental TDSLS signatures for acrylamide free radical polymerization. These signatures are fit with only two eligible parameters; M_w and the reaction rate constant α. Predictions concerning the evolution of M_w in a "dead-end" polymerization are also made and measured experimentally using an online monitoring method.

Introduction

The measurement of the intensity of light scattered from dilute solutions of polymers in equilibrium has been used for many years to characterize molecular mass, spatial dimensions, shapes, and virial coefficients.[1−3] Such total intensity measurements have often been termed "static light scattering" (SLS), which distinguishes the approach from the autocorrelation of fluctuations in scattered intensity, usually termed "dynamic light scattering" (DLS).[4]

While SLS is in widespread use for determining equilibrium properties of polymer solutions, there has been a growing emphasis on using SLS to follow nonequilibrium processes such as aggregation, phase separation, degradation, dissolution, and even the polymerization process itself. Recent approaches use continuous monitoring of the light scattered from solutions undergoing nonequilibrium processes, which is sometimes termed "time-dependent static light scattering" (TDSLS). TDSLS has been applied to gelation,[5] aggregation,[6−8] dissolution,[9] and other phenomena. In the area of polymer degradation, a significant "library" of TDSLS signatures has been derived and experimentally tested over the last 15 years.[10,11] TDSLS has also been used to investigate shear-induced fluctuations in semidilute polymer solutions.[12,13]

Monitoring polymerization reactions can elucidate kinetics and mechanisms, particularly for new areas of research, such as controlled radical polymerization (CRP).[14−16] In situ monitoring of monomer conversion is often accomplished by Raman,[17] infrared,[18−20] mid-infrared,[21] and near infrared spectroscopy.[22,23] In situ TDSLS has been reported in the dilute regime,[24] and for microemulsion-like polymerization.[25] Recently, automatic continuous online monitoring of polymerization reactions (ACOMP) was introduced,[26] which allows absolute and comprehensive characterization of polymer reactions in terms of monomer and comonomer conversion, weight-average molecular mass M_w, certain indices of polydispersity,[18,27] and intrinsic viscosity, as well as certain other features, depending on the type of reaction.

These latter methods are geared toward single sample measurements. In the early research phases for new polymerization reactions, where many reactions are simply to be screened for certain basic criteria, whence the most promising reactions are culled, it would be advantageous to have a coarser method that rapidly provides information on many samples. Simultaneous multiple sample light scattering (SMSLS) was recently introduced[28] and was used to make absolute M_w determinations of polymers and follow aggregation and degradation kinetics on independent samples.

In this work the focus is the fundamental relationship between the intensity of light scattered by solutions in which polymerization is occurring, and the intra- and interparticle characteristics of the evolving solution, as it passes from the dilute to semidilute regime. As such, scattering expressions thought to apply to dilute and semidilute solutions are investigated. A particularly novel feature of this work is that the transition from dilute to semidilute solution occurs in time as a result of polymerization reactions, whereas most concentration dependent studies are done on a discrete number of polymer solutions in equilibrium at different concentrations. In some ways, this work extends earlier in situ scattering measurements by Chu and Lee,[29] where the focus was on the combination of multiple detectors (static and dynamic light scattering, Raman spectroscopy) to obtain detailed characterization of polymerization. That work, however, did not present TDSLS signatures, nor explore their meaning in terms of the relationship between kinetics, M, A_2, and A_3. In this work, under a variety of well-established polymerization reaction models, some important classes of TDSLS signatures are established and then compared with experimental data. Data are normally fit with only two adjustable parameters: M_w and rate constant α. Novel results for "dead-end" polymerization are also presented.

* Corresponding author.
† Current address: Université de Rennes, 35042 Rennes, France.

10.1021/ma035835j CCC: $27.50
Published on Web 02/24/2004

General Theoretical TDSLS Signatures

As a polymerization reaction proceeds it will pass from the dilute regime into the semidilute regime and possibly into the concentrated regime. There are several different ways of estimating the concentration range of each regime. The "overlap concentration" c^* is one convenient measure of this and represents the concentration at which a solution passes from the dilute to semidilute regime. It can be approximated by $c^* \sim 1/[\eta]$, where $[\eta]$ is the polymer intrinsic viscosity. Semidilute solution behavior is expected roughly in the interval $1 < [\eta]c < 50$.[30] Another useful means of gauging the concentration regime is via the product A_2cM, where M is the mass of the polymer and A_2 its second virial coefficient. The existing light scattering expressions begin to diverge from each other for $A_2cM > 1$.

In the dilute regime the Zimm approximation[1] has consistently proven its validity

$$\frac{Kc}{I_R(c,q)} = \frac{1}{MP(q)} + 2A_2c + [3A_3Q(q) - 4A_2^2MP(q)(1 - P(q))]c^2 + O(c^3) \quad (1)$$

where $I_R(c,q)$ is the excess Rayleigh scattering ratio (cm^{-1}), c is the polymer concentration (g/cm^3), $P(q)$ the particle form factor, q is the amplitude of the scattering wave vector, $q = (4\pi n/\lambda)\sin(\theta/2)$, where θ is the scattering angle, $O(c^3)$ represents terms of order c^3 and higher, and K is an optical constant, given for vertically polarized incident light by

$$K = \frac{4\pi^2 n^2 (\partial n/\partial c)^2}{N_A \lambda^4} \quad (2)$$

where n is the solvent index of refraction, λ is the vacuum wavelength of the incident light, N_A is Avogadro's number, and $\partial n/\partial c$ is the differential refractive index for the polymer in the solvent. $Q(q)$ involves a sum of Fourier transforms of the segment interactions that define A_2.[1]

For a given polymer there is a relationship between A_2 and polymer mass M

$$A_2 = \frac{N_A}{2M^2}\frac{32\pi R_{eq}^3}{3} \quad (3)$$

where R_{eq} is the equivalent hard sphere radius of the polymer, no matter what its actual conformation. It is often possible to define a relationship between A_2 and M of the form

$$A_2 = aM^b \quad (4)$$

since R_{eq} is proportional to some power of M, depending on the conformation of the polymer. For a random coil with excluded volume, the theoretical value of b is -0.2.

The simplest available model for the third virial coefficient, A_3, is that of hard spheres, for which[31]

$$A_3 = \epsilon\frac{5MA_2^2}{8} \quad (5)$$

where $\epsilon = 1$ for hard spheres. For neutral polymers that resemble random coils, ϵ is usually found experimentally to range from 0.25 to 0.75[32−34] A lattice-model Monte Carlo study concludes that $\epsilon = 0.481$, universally, for long chain, neutral polymers,[35] whereas Stockmayer and Casassa[36] estimated $\epsilon \sim 0.40$, and $\epsilon = 0.43$ was found by renormalization group theory.[37] Recently, it was found that $\epsilon = 0.1$ over 2 orders of magnitude in ionic strength for sodium hyaluronate.[38] The effects of polydispersity on ϵ have not been treated, to the authors' knowledge.

For low enough concentrations that the c^2 term in eq 1 is negligible, and for $q^2\langle S^2\rangle_z < 1$, another, frequently used form of the Zimm equation is

$$\frac{Kc}{I_R(c,q)} = \frac{1}{M_w}\left(1 + \frac{q^2\langle S^2\rangle_z}{3}\right) + 2A_2c \quad (6a)$$

whereas the $q = 0$ limit of eq 1 gives a pure virial expansion expression for scattering

$$\frac{Kc}{I_R(c)} = \frac{1}{M_w} + 2A_2c + 3A_3c^2 + O(c^3) \quad (6b)$$

In the limit of $q = 0$, the following expression has been put forward to account for scattering through the crossover from dilute to semidilute solution:[39,40]

$$\frac{Kc}{I_R(c)} = 2A_2c\left[1 + 2\left(\frac{w_0}{p\Omega_\infty}\right)A_2Mc\right]^p + 3A_3c^2\left[1 - \frac{\Omega_{23}}{\Omega_\infty}\right]V(c) \quad (7)$$

Here

$$p = \frac{2 - 3\nu}{3\nu - 1}, \quad \text{where} \quad \nu = \frac{\partial(\ln\langle S^2\rangle^{1/2})}{\partial(\ln M)} \quad (8)$$

and

$$\Omega_{23} = \frac{A_2^2M}{A_3} = \frac{8}{5\epsilon} \quad (9)$$

and $w_0 = 0.75$ in order to recover the $q = 0$ limit of eq 1 given by eq 6b. Here Ω_{23} and Ω_∞ are measures of the second to third dimensionless virial coefficients; $\Omega_{23} \sim \Omega_\infty$ in the asymptotic limit. The second term in eq 7 is only significant if $A_2 \sim 0$ and the polymers are not very long, and $V(c)$ is unity at low c, and approaches another constant value at larger c.

For a good solvent, the Flory value of ν is 0.6, which gives $p = 0.25$. The more exact perturbative treatment[41] gives $\nu = 0.583$, for which $p = 0.335$. For $\nu = 0.5$, the Θ solvent limit, $p = 1$, and although A_2 is expected to be zero in this limit, eq 7 recovers the $q = 0$ form of eq 1.

Figure 1 shows the product KcM/I_R vs the dimensionless variable A_2cM, both for the virial expansion of eq 6b and for eq 7. In the latter case, various values of p are used. Roughly a factor of 2 difference appears in the extremes between eqs 6b and 7 with $p = 0.25$.

In this work, because the goal is to find distinct, major trends in TDSLS signatures, the problem of polydispersity, and how it affects the actual averages of each quantity measured, will be ignored. Unless multimodal populations are produced in the polymerization reactions, the current approach should be an adequate first approximation.

As will be shown in the results, the virial expansion of eq 6b provides better matches to the experimental

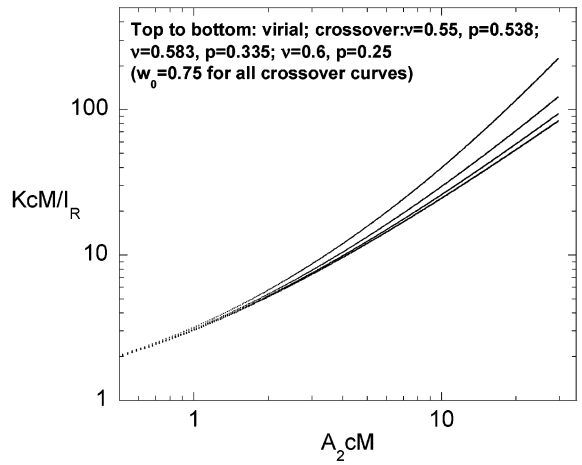

Figure 1. KcM/I_R vs the dimensionless quantity A_2cM for both the virial expansion, eq 6b in the $q = 0$ limit, and for the crossover expression, eq 7, for various values of ν and hence p.

data than the crossover expression of eq 7, no matter what value of p is used. As such, this work focuses on eq 6b, although comparisons with eq 7 are also made below.

The primary data furnished by TDSLS is $I_R(c,q,t)$. The useful form of eq 1, at $q = 0$ and with explicit time dependence of each parameter, is

$$I_R(t) = \frac{K(t)c(t)}{\frac{1}{M_w(t)} + 2A_2(t)c(t) + 3A_3(t)c(t)^2 + ...} \quad (10)$$

The above considerations mean that if, experimentally, the power law of eq 4 is established for a polymer, and the value of ϵ in eq 5 is found, then M_w will be the only free parameter in eq 10 above.

Theoretical TDSLS Signatures for Chain Growth Polymerization Reactions

Moving eq 10 into the time domain requires models for polymer concentration $c = c(t)$, and $M_w = M_w(t)$. Such time dependence will be based on the particular polymerization reaction involved. Here, chain growth polymerization, as exemplified by free radical polymerization in the absence of chain transfer, is considered. A powerful approximation exists for free radical polymerization; the quasi-steady-state approximation (QSSA).[42] In this it is assumed that the rate of production of propagating free radical R is balanced by its rate of consumption; i.e., $d[R]/dt = 0$, so that

$$[R] \cong \sqrt{\frac{Fk_d[I_2]}{k_t}} \quad (11)$$

where $[I_2]$ is the concentration of initiator, F is the fractional efficiency of the initiator, k_d is the initiator decomposition rate constant, and k_t is the termination rate constant.

In the limit where the lifetime of the initiator is much longer than the time for complete monomer conversion, a first-order decay of [m] is obtained

$$[m](t) = [m]_0 e^{-\alpha t}, \quad \alpha = k_p[R] \quad (12)$$

[m] is the molar monomer concentration and k_p is the polymer propagation rate constant. The monomer conversion $f(t)$, is defined as

$$f(t) = 1 - \frac{[m](t)}{[m]_0} \quad (13)$$

The kinetic chain length ν is the ratio of the probability of propagation to that of termination. It is the equal to the instantaneous number-average degree of polymerization $N_{n,inst}$, when chain transfer is absent

$$N_{n,inst} = \frac{k_p[m]}{k_t[R]} \quad (14)$$

Because [R] remains constant in this limit, the molecular weight (degree of polymerization times monomer mass) decreases with conversion f

$$M_{n,inst}(f) = M_{n,0}(1 - f) \quad (15)$$

and the cumulative, weight-average mass, measured directly by TDSLS, is given by

$$M_w(f) = M_{w,0}(1 - f/2) \quad (16)$$

where $M_{n,0}$ and $M_{w,0}$ are the initial number and weight-average masses.

ACOMP analysis of acrylamide polymerization found that first-order conversion kinetics were obeyed to a good approximation over a wide range of polymerization conditions.[43] In these same experiments, it was found that eq 16 was obeyed over most of the conversion. In several cases, however, very long chains were initially produced over early conversion before falling, roughly exponentially, to the form of eq 16 for the remainder of the conversion. ACOMP studies of vinylpyrrolidone polymerization have shown both $M_w(t) =$ constant and eq 16 behavior, depending on the details of the reaction.[18]

Figure 2a shows computed TDSLS signatures using eq 10 for free radical polymerization and first-order kinetics under three different scenarios: (1) low concentration of monomer (0.0036 g/cm^3) and constant $M_w(t) = 10^6$; (2) 0.036 g/cm^3 concentration and constant $M_w(t) = 10^6$; (3) the latter concentration, but with $M_w(t)$ decreasing according to $M_w(t) = 10^6 + 6 \times 10^6 \exp(-1.25\alpha t)$. The $M_w(t)$ profiles are shown in Figure 2c. In the first case, scattering is dominated by M_w and then by A_2, with no appreciable A_3 effects, since the solution is dilute enough. With a more concentrated solution, a maximum in $I_R(t)$ is reached followed by a decline to a plateau. In the case of the exponentially decreasing $M_w(t)$, there is actually a minimum after the peak, followed by a gradual rise. In all cases $K(t)$ is taken as constant in eq 10, since there is no appreciable change in $\partial n/\partial c$ for long chain polymers of varying length.

Although a detailed exploration of deviations from ideal first-order conversion is beyond the scope of this paper it is noted that certain common deviations, such as initial competition between impurities (e.g., oxygen) and monomers for radicals, lead to a delay in establishing near-ideal kinetics, and the conversion vs time shows a distinct, initial upward curvature with an inflection point.[43] This leads to initial upward curvature in I_R, which will never occur otherwise for ideal free radical polymerization. Hence, this type of deviation

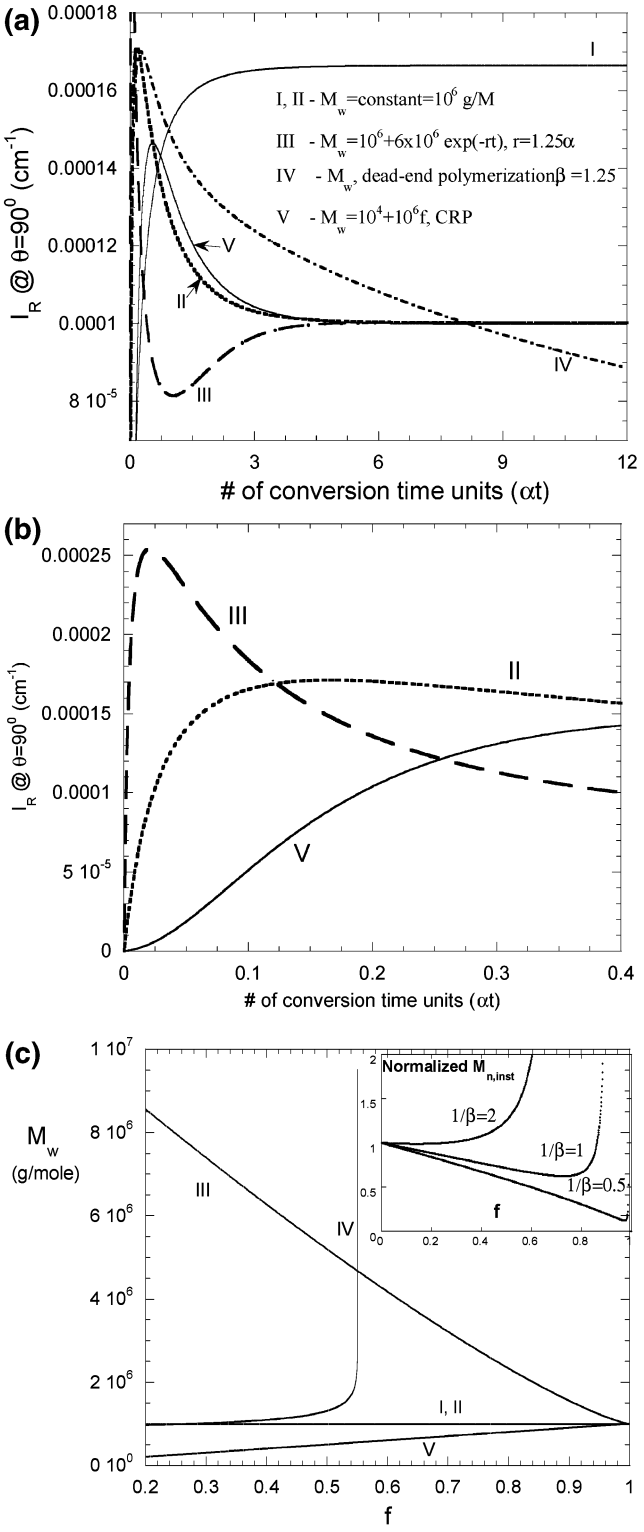

Figure 2. (a) TDSLS signatures from eq 10 for first-order conversion, according to different theoretical and experimentally encountered behaviors for $M_w(t)$. (b) Enhanced x-scale of Figure 1a shows markedly different early conversion behavior for different polymerization scenarios. (c) $M_w(f)$ curves leading to each signature in Figure 1a. The inset shows the dramatic effect that β has on the evolution of $M_{w,inst}(f)$ in dead-end polymerization.

from ideality, and probably others, should be detectable by the methods presented here.

In another important limiting case of the QSSA, the "dead-end",[44] all the initiator is used up before all monomer has been converted to polymer. A first-order decay of [R] leads to an expo-exponential decrease in $[m](t)$

$$[\mathrm{m}](t) = [\mathrm{m}]_0 \exp\left[\frac{2Ak_\mathrm{p}}{k_\mathrm{d}}(\mathrm{e}^{-k_\mathrm{d}t/2} - 1)\right], A = \sqrt{\frac{Fk_\mathrm{d}I_0}{\mathrm{k_t}}} \tag{17}$$

Likewise, the instantaneous number-average kinetic chain length is given by

$$\nu_\mathrm{n} = \frac{k_\mathrm{p}[\mathrm{m}]_0 \exp\left[\frac{2\mathrm{A}k_\mathrm{p}}{k_\mathrm{d}}(\mathrm{e}^{-k_\mathrm{d}t/2} - 1)\right]}{k_\mathrm{t}A\mathrm{e}^{-k_\mathrm{d}t/2}} \tag{18}$$

Equation 18 allows for the possibility that the molecular mass *increases* during the reaction, as opposed to the linear decrease vs f given by eq 15.

Equation 18 can be expressed in terms of f as

$$\nu_\mathrm{n} = \frac{1-f}{1+\beta\ln(1-f)}, \beta = \frac{k_\mathrm{d}}{2Ak_\mathrm{p}} \tag{19}$$

Equation 19 shows that the instantaneous kinetic chain length diverges to infinity as the limiting conversion f_c is reached, where

$$f_\mathrm{c} = 1 - \exp\left(\frac{-2Ak_\mathrm{p}}{k_\mathrm{d}}\right) \tag{20}$$

The effect of β on the behavior of the instantaneous mass is so striking that examples of the predicted QSSA behavior are shown in the inset to Figure 2c.

The predicted cumulative $M_w(f)$, which is measured directly by TDSLS, is

$$M_\mathrm{w}(f) = \frac{-1.5\int\left(\frac{x'}{1+\beta\ln x'}\right)\mathrm{d}x'}{1-x} \tag{21}$$

where $x = 1 - f$, and it is assumed, as is done by other authors, that $M_{w,inst}(f) = 1.5\ M_{n,inst}(f)$. This can be transformed into the form of the more familiar exponential integral function

$$M_\mathrm{w}(f) = \frac{\frac{\mathrm{e}^{-2\beta}}{\beta}\int_0^f e^{\frac{2z/\beta}{z}}\mathrm{d}z}{f} \tag{22}$$

Like the instantaneous chain lengths, $M_w(f)$ also diverges at f_c.

Although the cumulative number-average $M_n(f)$ is not directly measured by TDSLS, it can be measured by GPC

$$M_\mathrm{n}(f) = \frac{-f}{\ln(1-f)\left[1+\frac{\beta}{2}\ln(1-f)\right]} \tag{23}$$

Remarkably, $M_n(f)$ does not diverge to infinity at f_c, unlike the other instantaneous and cumulative averages.

Tobolsky et al.[45] derived expressions for polydispersity indices in the case of chain transfer in the dead-end

scenario, but did not mention the possibility of a divergent mass, nor did they perform experiments. Wooster generalized dead end polymerization theory to include reactions of different order that compete between propagation and termination reactions, and hence can deviate from Tobolsky's and the above treatment.[46]

Figure 2a includes a TDSLS signature according to eqs 10 and 22 for $M_W(f)$. Because of the divergent mass, $I_R(t)$ tends toward zero, rather than reaching a plateau, as in the other cases.

Finally, the signature of a typical controlled radical polymerization (CRP) is shown, curve 5 in Figure 2a, which yields an inflection point before the maximum is reached, which can be seen in Figure 2b. In CRP there are a finite number of propagating radicals that are reversibly "capped" by a compound, such that they become active for brief intervals and add monomer, so that each active chain lasts the life of the entire monomer conversion process, leading to polymer mass that increases linearly with f.

Experimental Materials and Methods

Ultrapure electrophoresis grade acrylamide (Aam) and potassium persulfate (KPS, 99% minimum purity) were from Polysciences, Inc. and *N,N,N′,N′*-tetramethylethylenediamine (TMEDA, 99% minimum purity) was from Spectrum Quality Products, Inc. All reagents were used without further purification. Solutions of each reagent were made in ultrapure deionized water and purged under nitrogen. Aam concentrations were from 0.0039 to 0.035 g/mL and concentrations used for KPS and TMEDA were from 0.011 to 0.1 mol/L. The solutions were filtered through a 0.22 μm Millipore filter. First, 3 mL of monomer solution was injected in each reactor, and then 0.1 mL of KPS was injected and finally 0.1 mL of TMEDA solution. The ratio of the catalytic initiator system KPS/TMEDA in each reactor was 1:1 in mol. The polymerization reactions were carried out, eight at a time in the SMSLS device, at $T = 25$ °C under constant nitrogen flow.

SMSLS measurements were made at a scattering angle of 90°, with an incident, vertically polarized laser beam at 677 nm, in vacuo, and removable, square borosilicate cuvettes were used for the reactions and in situ SMSLS monitoring. There was 3.2 mL of reacting liquid in each cuvette, which was constantly stirred. The scattering volume was on the order of 10 nL, and together with recognition of any spurious scattering peaks in the data, this allowed for virtually complete elimination of scattering due to "dust" and other impurities. While more scattering angles would be preferable for extrapolations to $q = 0$, the current design geometry did not allow this. Hence, while this work is focused on the extraction of reaction rate constants and average polymer masses during polymerization, the current apparatus does not permit structural determinations of the polymer to be made.

Measurements of A_2 and A_3 were made by using a variety of Polyacrylamide (PAAm) endproducts using automatic continuous mixing, ACM. This method has been previously detailed,[47] and involves using a mixing pump to make continuously changing gradients of the various components in a multicomponent solution, so that a continuous record of both light scattering and viscosity is obtained over the entire gradient. In these ACM experiments full angular extrapolations to $q = 0$ from multiangle light-scattering measurements were made in determining A_2 and A_3.

End products of various Aam reactions were also analyzed by gel permeation chromatography (GPC), on a system comprising an Agilent 1100 isocratic pump, an OHpak Shodex 806 HQ column, a Shimadzu RID-10a refractometer, a Brookhaven Instruments Corporation BI-M_wA multiangle light scattering detector, and a home-built single capillary viscometer.

ACOMP was used to verify the predictions for dead-end reactions above using polystyrene. Because reactions for finding TDSLS polymerization signatures were carried out at room temperature with SMSLS, it was not possible to create a dead-end reaction. The ACOMP results below, however, establish the basis for reasonably expecting the predictions for dead-end reactions from the last section to hold true.

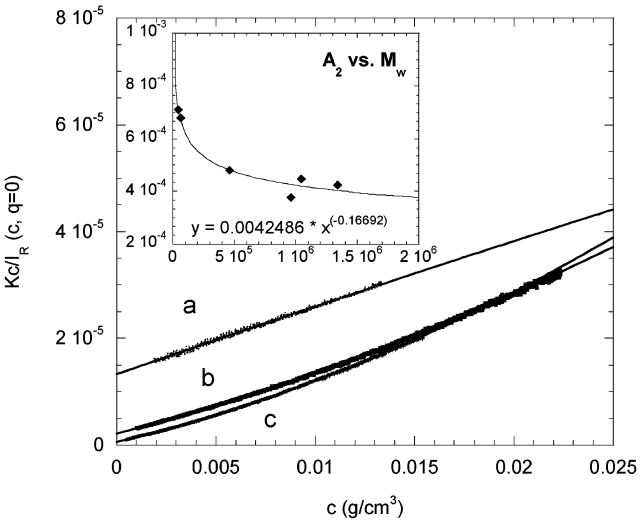

Figure 3. Typical ACM results for PAAm. The values of $Kc/I_R(c,q)$ are extrapolated to $q = 0$ and plotted vs c, whence M, A_2 and A_3 are obtained. The inset shows A_2 vs M.

Table 1. Subset of ACM Experiments Shown in Figure 3

expt	$M_w(q = 0)$	$A_2(q = 0)$	$A_3(q = 0)$	M_w(GPC)
a	74 800	6.30×10^{-4}		66 100
b	463 000	4.80×10^{-4}	0.0059	370 000
c	1 829 000	4.46×10^{-4}	0.0086	1 044 800

ACOMP is based on the automatic, continuous extraction of a very small amount of reactor fluid, which is mixed with a large amount of solvent, such that a continuous, dilute stream of sample passes through a detector train, here comprised of a home-built seven-angle light-scattering device, a Shimadzu SPD10-AVVP ultraviolet spectrophotometer for monitoring the conversion of styrene monomer into polymer, and a Waters 410 refractometer to monitor total solute. The ACOMP system has previously been described in detail but was modified here to have low pressure and high pressure mixing stages, allowing high viscosity reactor liquid to be continuously sampled. THF was used as the diluent. The dilute stream reaching the detector contained 0.77% by mass of combined monomer and polymer.

For the ACOMP dead-end experiments, styrene (99%), ethylbenzene (99%), and *tert*-amylperoxy 2-ethylhexyl carbonate (Luperox TAEC, 92%) were purchased from Aldrich. All reagents were used without further purification. Polymerization reactions were carried out in a jacketed reactor connected to a circulating oil bath and equipped with a mechanical stirrer and a temperature probe. A mixture of 94 wt % of styrene and ethylbenzene (200 mL) was poured in the reactor, purged with nitrogen at room temperature for 1 h and then heated to 110 °C. Then 500 ppm of Luperox TAEC was injected into the hot reaction mixture, and the polymerization reaction was carried out at 120 °C.

Experimental Results

ACM Determinations of A_2 and A_3. Figure 3 gives examples of ACM data used to determine A_2 and A_3. The inset to Figure 3 shows A_2 vs M_w, which gave

$$A_2 = 0.00425 M_w^{-0.167} \qquad (24a)$$

M_w is used in eq 24a, whereas eq 4 is for monodisperse fractions. Table 1 gives the values of M_w, A_2, and A_3 for the subset of ACM experiments shown in Figure 3.

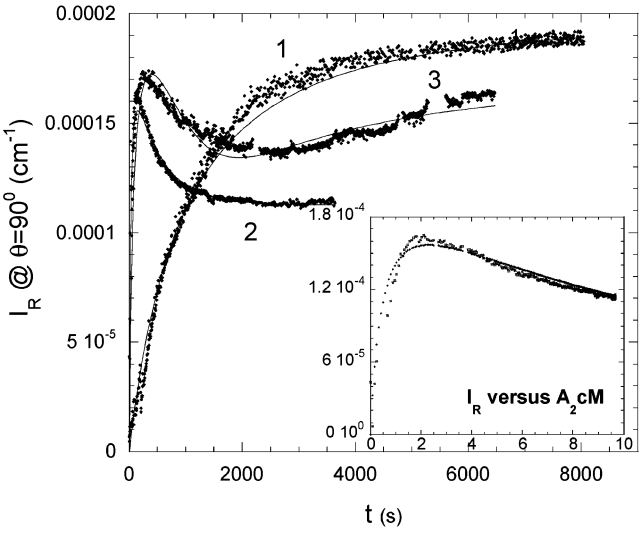

Figure 4. Experimental TDSLS results for $I_R(t)$ for Aam polymerization reactions, with fits according to eq 10. In the inset to the figure, I_R is plotted vs A_2cM (experiment no. 2 only) in order to show the pertinence to the semidilute concentration solution regime.

The strong upward curvature of $Kc/I_R(c, q = 0)$ is a direct consequence of A_3 in eq 6b, which allows this latter to be computed from ACM data. From A_2 and A_3 results it was found that $\epsilon = 0.095 \pm 0.03$. Up to 0.025 g/cm^3, there is no evidence at all for A_4 effects, so they have not been considered in the following analysis. While including A_4 in eq 3 is straightforward, its relationship to A_3, and hence A_2, for real coil polymers is not well established and must certainly deviate strongly from Boltzmann's A_4 expression for hard spheres.

The intrinsic viscosity data from GPC yielded

$$[\eta]_w = 0.0041 M_w^{0.81} \tag{24b}$$

Using the usual approximation that the semidilute concentration $c^* \sim 1/[\eta]_w$, $c^* = 0.020$ g/cm^3 for $M_w = 10^5$ and 0.003 g/cm^3 at $M_w = 10^6$. Most of the experiments were done at a beginning Aam concentration of 0.035 g/cm^3, which means they were well into the semidilute regime by the time final conversion was reached.

TDSLS Signatures from in Situ SMSLS Monitoring of Acrylamide Polymerization. Of the five families of curves shown in Figure 2a, three were found experimentally to represent all the eight simultaneous reactions in an SMSLS experiment. Typical curves exemplifying the different types of signatures are shown in Figure 4, together with fits according to eq 10 and first-order monomer conversion kinetics,

$$c(t) = c_{m,0}(1 - e^{-\alpha t}) \tag{25}$$

where $c(t)$ is the polymer mass concentration (g/cm^3), and $c_{m,0}$ is the initial monomer concentration.

Table 2 compares the M_w values from the fits to the TDSLS data to those obtained by GPC for a total of six of the experiments. The agreement is quite good. Moreover, TDSLS yields the rate constant for assumed first-order conversion, which, of course, the GPC approach cannot. The general trends expected for free radical polymerization are found in Table 2. Namely, M_w increases with an increasing ratio of monomer to initiator, and the rate constant α increases with increasing initiator concentration.

In the inset to the Figure 4, I_R is plotted vs A_2cM (experiment no. 2 only) in order to show the crossover into the semidilute regime. Both experimental data and the curve fit (using the time-dependent virial expression, eq 10) are included. When two or more fitting parameters are used, there is a family of parameter values that yield the same root-mean-square error. Hence, confidence intervals were established by numerically computing grids of points and finding the locus of parameter points within a given rms error interval, where the squared error at each point was $(I_{R,calcd} - I_{R,exptl})^2/I_{R,exptl}^2$. Examples are shown in Figure 5, parts a and b. Figure 5a shows contours of points for average root-mean-square errors of 2.2, 2.7, and 4.7% where ϵ is fixed to its experimental value of 0.095 and M and α are the two adjustable parameters. In Figure 5b, parameters yielding an average error less than 4% are shown, computed for values of $\epsilon = 0.08$, 0.095 (the average experimental value), and 0.11, where M and α are again taken as the two adjustable parameters.

The time derivative of $I_R(t)$ (calculated from eq 10) gives a relationship between the initial value of $dI(t)/Kdt$, the initial monomer conversion rate α and M_w

$$\alpha = \frac{\left.\frac{dI_R(t)}{dt}\right|_{t=0}}{Kc_{m,0}M_w} \tag{26}$$

At the maximum of $I_R(t)$ all time dependence vanishes and a "snapshot" of the system at that point appears, where

$$c_{@I_{max}} = \frac{1}{\sqrt{3A_3 M_{w@I_{max}}}} \tag{27}$$

Interestingly, if $c_{@I_{max}}$ can be determined, as described below, then $M_{w@I_{max}}$ can be determined, if A_2 is known and eq 5 is used for the relationship between A_2 and A_3. $M_{w@I_{max}}$ is hence obtainable in this way even when $I_R(t)$ is expressed in completely arbitrary units $I(t)$, as opposed to reducing raw $I(t)$ to the absolute $I_R(t)$.

The value of I_R/K at the maximum allows for an internal consistency check of the values and models used. Namely, if eq 5 for A_3 is used in conjunction with $c_{@I_{max}}$ in the above, and this is substituted back into eq 10, then

$$\left.\frac{I_R(t)}{K}\right|_{max} = \frac{1}{2A_2\left(1 + \sqrt{\frac{15\epsilon}{8}}\right)} \tag{28}$$

Table 2 summarizes the various aspects of the TDSLS signature analysis, including fits of the SMSLS $I_R(t)$ at $\theta = 90°$, according to eq 10, to find the average value of the apparent M_w at 90°, denoted by $M_{w,90}$, and the range of $M_{w,90}$ using the error contour analysis, radius of gyration corrected values of M_w, conversion rate constants α, GPC values of M_w and the values of M_w obtained by GPC at $\theta = 90°$, without extrapolation to $\theta = 0°$, i.e., $M_{w,GPC,90}$. The experimental value of $\epsilon = 0.095$ is used in the fits.

The columns "$M_{w,90}$(I_R fit)" and "α(I_R fit)" are the values found from nonlinear fits to $I_R(t)$ according to eq 10, with the A_2/M_w relationship of eq 24a, using ϵ as a

Table 2. Summary of SMSLS Experiments, Fitting Parameters (M_w and α),[a] and GPC Values

			$M_{w,90}$(I_R fit)			M_w(I_R fit) corr by eq 30			α (1/s) (I_R fit)		
expt	$[m_0]$ (M)	$[I_0]$ (M)	av	range for 4% rms error	$M_{w,GPC,90}$	av	range for 4% rms error	M_w(GPC)	av	range for 4% RMS error	α (1/s) (I_R in slope)
1	0.125	3.4×10^{-4}	6.8×10^5	6.0×10^5 1.0×10^6	5.5×10^5	9.3×10^5	7.9×10^5 1.6×10^6	7.8×10^5	1.9×10^{-4}	1.0×10^{-4} 2.5×10^{-4}	1.0×10^{-4}
2	0.5	3.1×10^{-3}	5.8×10^5	4.0×10^5 1.0×10^6	5.6×10^5	7.6×10^5	4.8×10^5 1.6×10^6	1.1×10^6	1.7×10^{-3}	1.0×10^{-3} 4.0×10^{-3}	8.0×10^{-4}
3	0.5	7.8×10^{-4}	6.7×10^5	4.0×10^5 1.0×10^6	1.1×10^6	9.1×10^5	4.8×10^5 1.6×10^6	2.1×10^6	1.1×10^{-3}	3×10^{-4} 1×10^{-3}	4.0×10^{-4}
4	0.125	3.1×10^{-3}	1.1×10^5	1.0×10^5 1.3×10^5	2.42×10^5	1.1×10^5	1.0×10^5 1.3×10^5	3.3×10^5	2.7×10^{-3}	2.2×10^{-3} 5.6×10^{-3}	1.3×10^{-3}
5	0.125	7.8×10^{-4}	3.8×10^5	3.0×10^5 5.5×10^5	3.9×10^5	4.6×10^5	3.4×10^5 7.1×10^5	4.8×10^5	3.7×10^{-4}	2×10^{-4} 6×10^{-4}	2.1×10^{-4}
6	0.0055	3.4×10^{-4}	1.6×10^5	1.2×10^5 2.1×10^5	1.3×10^5	1.7×10^5	1.3×10^5 2.3×10^5	1.4×10^5	3.4×10^{-4}	2×10^{-4} 5.8×10^{-4}	2.0×10^{-4}

[a] M_w and α fitting range are given for an error up to 4%. $\epsilon = 0.095$ was used throughout. Concentration values at $I_{R_{max}}$ were computed as follows: 7.8×10^{-3} g/cm^3 (experiment no. 2) and 8.3×10^{-3}g/cm^3 (experiment no. 3), respectively.

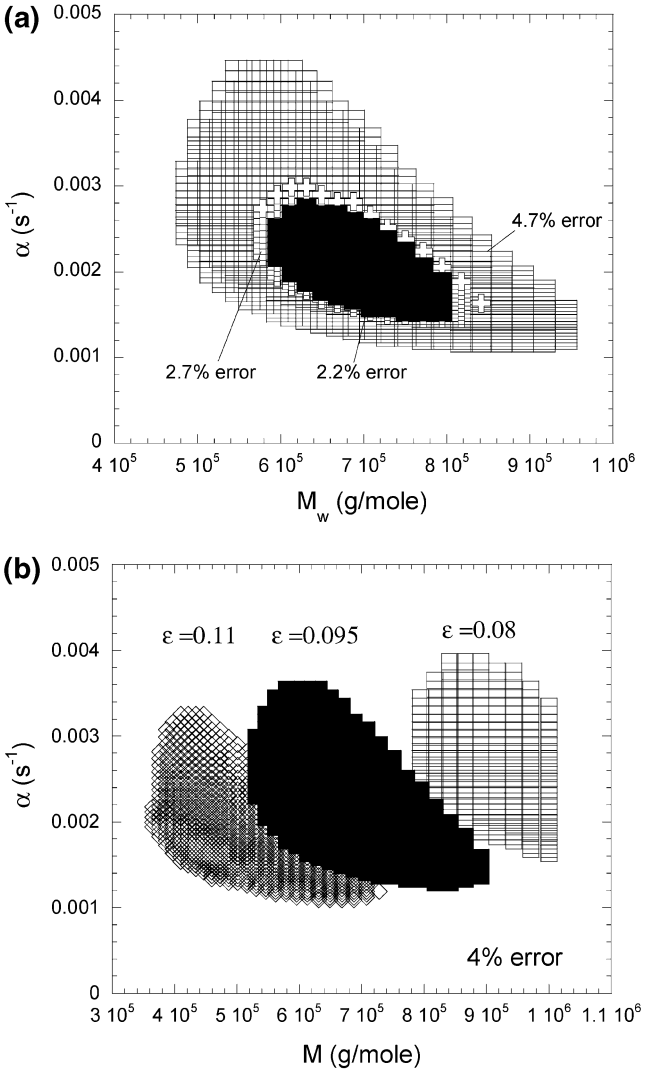

Figure 5. (a) Rms error contours for curve 2 in Figure 4, when M_w and α are the two adjustable parameters and $\epsilon = 0.095$ (its experimental value). (b) Rms error contours for curve 2 with M and α, using three different values of ϵ: 0.095 (the average experimental value), 0.08, and 0.11.

fitting parameter (since its experimental average value of 0.095 has a large error bar). The ranges of $M_{w,90}$ values shown underneath the top values in the "$M_{w,90}$-(I_R fit)" column are those found for rms fitting errors less than 4%.

A first order correction for the values of $M_{w,90}$ from the SMSLS experiments was also made with the relationship between $\langle S^2 \rangle$ and M established by the GPC measurements using fits to multiangle light-scattering detection and eq 6a:

$$\langle S^2 \rangle^{1/2} \text{ (cm)} = 1.92 \times 10^{-9} \, M^{0.60} \qquad (29)$$

The agreement between M_w corrected this way, using the fitted $M_{w,90}$ as M in eq 26, was good. To obtain M_w from $M_{w,90}$, the correction is

$$M_w = M_{w,90}(1 + 3.72 \times 10^{-8} M_{w,90}{}^{1.2}) \qquad (30)$$

The correction amounts to 4% for $M_{w,90} = 1 \times 10^5$, 25% at $M_{w,90} = 5 \times 10^5$, and 59% at $M_{w,90} = 1 \times 10^6$. It is pointed out that R_g in the semidilute regime may decrease,[30] so that the above expression may overcorrect for the R_g effect later in conversion. At any rate, it is clear that the method is less accurate when larger M_w polymers of a given type are involved.

The fit in Figure 4 for curve 3 requires a special explanation. Since it resembles signature III in Figure 1a, its form is presumably due to a large initial M_w that decreases rapidly as conversion proceeds. The fit involved $M_{w,90}$ decaying according to $M_{w,90} = M_{w,final} + M_0 \exp(-rt)$. The best fit gave $M_{w,final}$ in the range 4×10^5 to 8.5×10^5 g/mol, M_0 in the range 5×10^6 to 9×10^6 g/mol, α in the range 1.2×10^{-4} to 3×10^{-5} s^{-1}, and r from 18α to 90α, with ϵ ranging from 0.04 to 0.15. The large value of r compared to α implies that the early very high masses quickly reduce to the much smaller value of M_0. Such behavior for Aam free radical polymerization can be seen in Figure 3 of ref 43. Because there are five adjustable parameters in the fit to Figure 4 ($M_{w,final}$, M_0, r, α, ϵ), however, the ranges of each are quite wide and their uncertainties great. This is the usual price paid when increasing numbers of adjustable parameters are used to fit data. If the rise in $I_R(t)$ in curve 3 in Figure 4 after $t = 2000$ s is ignored, and the data fit more conservatively with only three parameters (average M_w, α, ϵ), then the values shown in Table 2 are obtained. In this case M_w falls within the range of the five-parameter fit, but α is an order of magnitude larger. This is probably because r in the five parameter fit absorbs most of the rapid time behavior in $I_R(t)$. Thus, it is possible to at least detect a certain phenomenon, such as large initial M_w, with the TDSLS signature,

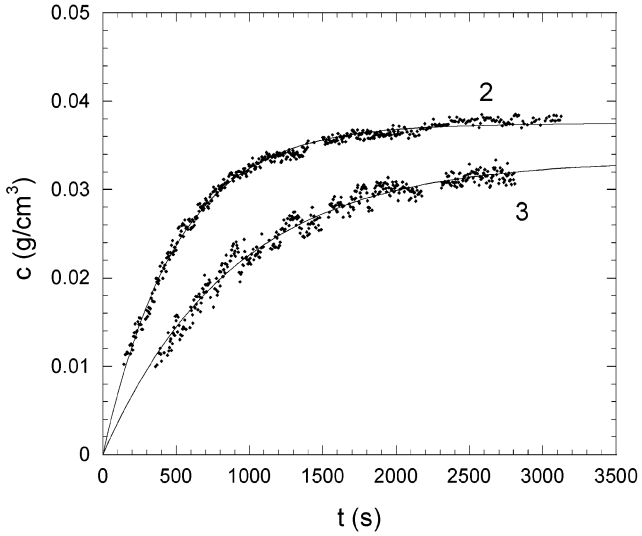

Figure 6. $c(t)$ extracted from experiments 2 and 3 according to eq 31.

without always being able to get good quantitative information on the phenomenon.

Figure 6 shows $c(t)$, extracted from experiments 2 and 3 in Figure 4, according to

$$c(t) = \frac{1}{6A_3}\left(\frac{K}{I_R(t)} - 2A_2\right) + \left(\frac{\left(2A_2 - \frac{K}{I_R(t)}\right)^2}{36A_3^2} - \frac{1}{3A_3M_w}\right)^{1/2} \quad (31)$$

It is interesting to see both how well the kinetics actually follow the first-order prediction above (first-order fits are shown, and rate constants from the fit to eq 31 are shown in Table 2) and how this monotonic $c(t)$ is contained within the more complex parent signature $I_R(t)$. While the first-order behavior of $c(t)$ is "built into" the fit to $I_R(t)$, and hence the parameter ϵ in eq 31 and the value of M_w used to find A_2 according to eq 24a, deviations from first order should show up much more clearly in the extracted curve of $c(t)$ in eq 31, as opposed to in the fit to $I_R(t)$. The rate constant α is not used in eq 31, allowing for a subsequent cross-check on its value. It is noted that first-order kinetics for similar acrylamide polymerization reactions have been reported.[43]

Results using the Crossover Scattering Expression (Eq 9). In principle, eq 7, the crossover light-scattering expression, would be expected to be more appropriate for analyzing the experimental data. Figure 7 shows fits to data curve 2 in Figure 4 using both eq 6b and the crossover expression, eq 7. Interestingly, the virial expansion gives the best fit, although eq 7 also gives reasonable fits, if ϵ is left as a free parameter, but there is a progressive divergence from the data as p approaches its limiting value of 0.25. Table 3 shows the results of the crossover expression (eq 7) for α and M, for both the case of $\epsilon = 0.1$ and the case when ϵ is left as a fitting parameter. In the latter case, the fits to the data are much better, but at the expense of finding values of ϵ that are far from the experimental value. Whether this is due to polydispersity effects, the unusually low value of ϵ, or some other reason is not clear at this stage.

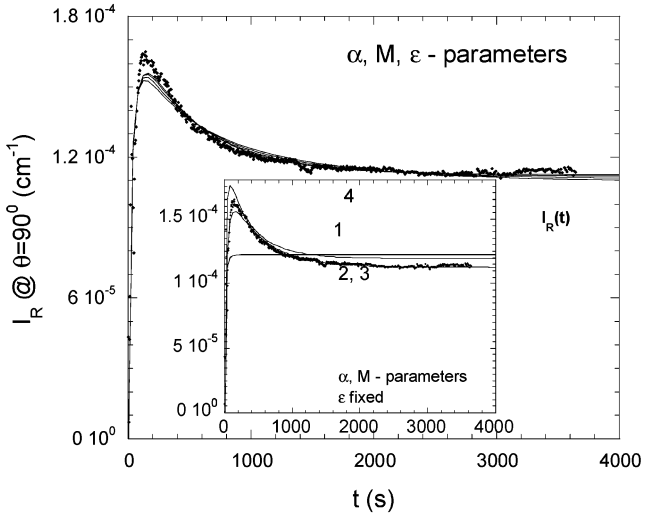

Figure 7. Fits to experimental curve 2 (Figure 4) using both eq 6b and the crossover expression, eq 7, ϵ chosen as a parameter as M and α. In the inset, the same equations used to fit data, at ϵ fixed.

Table 3. Results of the Crossover Expression (Eq 7) Applied to Data from Experiment No. 2 for α and M, for both the Case of $\epsilon = 0.1$ and the Case When ϵ Is Left as a Fitting Parameter[a]

ϵ	p	α (s^{-1})	M (g/mol)
0.397	0.25	8.39×10^{-4}	1.24×10^6
0.224	0.335	1.13×10^{-3}	9.086×10^5
0.138	0.538	1.48×10^{-3}	6.96×10^5
0.1	0.25	2.15×10^{-2}	1.089×10^6
	0.335	1.91×10^{-2}	1.1149×10^6
	0.538	2.1×10^{-3}	5.157×10^5
	virial (eq 6b)	1.7×10^{-3}	5.8×10^5

[a] As a comparison, α and M values from the virial expression are included in the last raw of the table. M_w from GPC (90°): 5.6×10^5 g/mol.

In the inset to the figure the same fits are applied to experimental data, keeping ϵ fixed. In this last case, the curve fits from the crossover equation are far away from data; only for $p = 0.538$ (curve 4) the fit curve gives reasonable results; as p approaches 1, the fits look more accurate and the results are comparable with those from the virial expansion. Curves 2 and 3 are obtained using the crossover equation with $p = 0.25$, respectively 0.335, while the virial expression provides curve 1 (the best fit).

Hence, while eq 7 may represent a conceptually more satisfying way to approach the understanding of scattering from semidilute solutions, it has less practical utility, at least in this instance, and gives values of M less in accord with the GPC values than the virial expression. It is advisable to continue comparing the results of both eq 6b and eq 7, or variants thereof, as more experiments are performed for different polymerization reactions.

ACOMP Monitoring of a Dead-End Free Radical Polymerization. Finally, although it was not possible to cause a dead-end reaction with the current room-temperature reactions used in the SMSLS device, results on a dead-end reaction for polystyrene at $T =$ 110 °C were obtained using ACOMP. The authors are unaware of any published data corroborating the divergent instantaneous and cumulative weight-average masses predicted by eqs 19 and 22, above. Figure 8 shows concentration vs t, with the expo-exponential fit

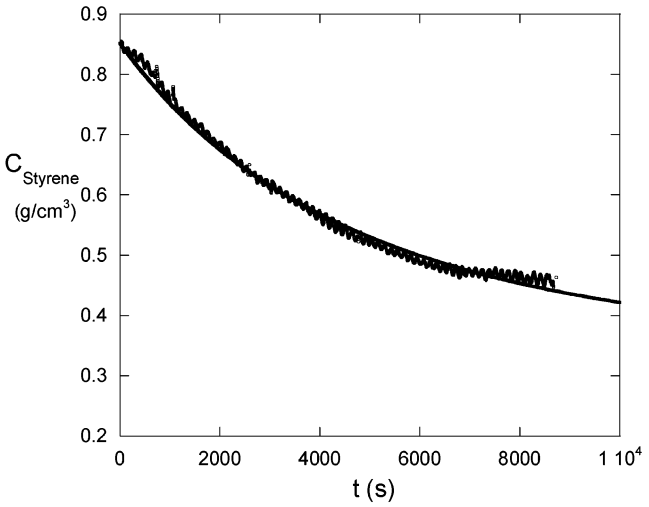

Figure 8. Experimental ACOMP results for dead-end polymerization; conversion vs t, with solid line fit according to eq 17, which yielded $\beta = 3.5$ (defined in eq 19).

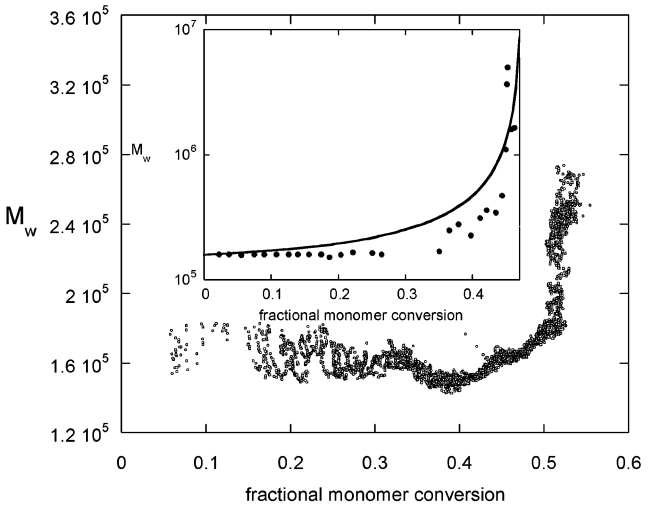

Figure 9. Experimental ACOMP results for dead-end polymerization: $M_w(f)$, the cumulative mass in the reactor measured directly by ACOMP. The inset shows $M_{w,inst}(f)$ obtained from eq 32, with a solid line fit to eq 19.

according to eq 17. The dead end is seen to be approached in the data at c_m about 0.43 g/cm^3, and the fit predicts the dead end at 0.35 g/cm^3.

Figure 9 shows $M_w(f)$, the cumulative weight-average mass of polymer in the reactor, measured directly by ACOMP. The inset shows the instantaneous value of M_w, obtained according to ref 27

$$M_{w,inst}(f) = M_w(f) + f\frac{dM_w}{df} \tag{32}$$

where the continuous $M_w(f)$ data were broken into discrete intervals for computing $M_{w,inst}(f)$. Also shown is the fit to $M_{w,inst}$ according to eq 19, which yielded $\beta = 3.5$. Both $M_w(f)$ and $M_{w,inst}(f)$ show the divergence predicted by eqs 19 and 22 above.

Conclusions

TDSLS signatures of solutions undergoing chain growth polymerization reactions and passing from the dilute to the semidilute solution are obtained theoretically, and different families of qualitative signatures are found that distinguish between different kinetics and mechanisms of chain growth. In associated experiments, in which multiple reactions were carried out simultaneously with SMSLS, each signature found fell into one of three families of these signatures, examples of each of which were presented. The signatures contain semiquantitative information on both the kinetics of the reactions and the M_w of the polymers produced.

Only two parameters, the reaction rate constant α and the average polymer M_w, are normally needed to fit the data. Furthermore, qualitative deviations in the shape of the TDSLS signature during polymerization reactions may indicate problems with the reaction, deviations from ideal kinetics, or the appearance of unexpected phenomena.

It is interesting that the virial expansion (eq 6b) proves more robust in analyzing real data than the conceptually more elegant semidilute crossover scattering expression (eq 7). In more concentrated systems, at any rate, only the initial portion of the polymerization corresponding to the dilute and early semidilute regimes will be useful for the type of analysis developed here.

While SMSLS does not attempt to compete with absolute monitoring techniques, such as ACOMP, it nonetheless should prove useful for screening many reactions simultaneously, using the type of analysis presented here. Cross-checks on the values of M_w extracted from the TDSLS signatures are in reasonable agreement with GPC measurements made on end products of the same experimental samples.

It is left to future work to experimentally verify the predicted TDSLS signatures for CRP and dead-end reactions, and to develop further the library of TDSLS polymerization signatures for other types of reactions.

ACOMP data presented here bear out predictions presented concerning the divergence of cumulative and instantaneous weight-average polymer mass during dead-end reactions.

From a fundamental point of view, the scattering from the polymerization reactions provides a novel, nonequilibrium means for measuring the time-dependent effects of A_2 and A_3 as the solution passes from the dilute into the semidilute regime and provides a testing ground for different theories.

Acknowledgment. Support from Grants NSF CTS 0124006 and NASA NAG-1-02070 and NCC3-946 is gratefully acknowledged. E.M. acknowledges support from Atofina Corp., and advice on the Aam reactions from Bruno Grassl.

References and Notes

(1) Zimm, B. H. *J. Chem. Phys.* **1948**, *16*, 1093.
(2) Debye, P. *J. Phys. Colloid Chem.* **1947**, *51*, 18.
(3) Brown, W. *Light Scattering, Principles and Development*; Oxford Science Pub.: Oxford, England, 1996.
(4) Berne, B.; Pecora, R *Dynamic Light Scattering*; John Wiley & Sons: New York, 1976.
(5) Norisuye, T.; Shibayama, M.; Nomura, S. *Polymer* **1998**, *39*, 2769.
(6) Holthoff, H.; Egelhaaf, S. U.; Borkovec, M.; Schurtenberger, P.; Sticher, H. *Langmuir* **1996**, *12*, 5541.
(7) Wright, L. S.; Chowdhury, A.; Russo, P. *Rev. Sci. Instrum.* **1996**, *67*, 3645.
(8) Egelhaal, S. U.; Schurtenberger, P. *Rev. Sci. Instrum.* **1996**, *67*, 540.
(9) Michel, R. C.; Reed, W. F. *Biopolymers* **2000**, *53*, 19.
(10) Reed, C. E.; Reed, W. F. *J. Chem. Phys.* **1989**, *91*, 7193.
(11) Reed, W. F. *J. Chem. Phys.* **1995**, *103*, 7576.
(12) Hashimoto, T.; Fujioka, K. *J. Phys. Soc. Jpn.* **1991**, *60*, 356.
(13) Vanegmond, J. W.; Werner, D. E.; Fuller, G. G. *J. Chem. Phys.* **1992**, *96*, 7742.

(14) Matyjaszewski, K., Ed. *Controlled/Living Radical Polymerization. Progress in ATRP, NMP, and RAFT*. ACS Symposium Series 768; American Chemical Society: Washington DC, 2000.
(15) Benoit, D.; Chaplinski, V.; Braslau, R.; Hawker, C. J. *J. Am. Chem. Soc.* **1999**, *121*, 3904.
(16) Benoit, D.; Grimaldi, S.; Robin, S.; Finet, J.-P.; Tordo, P.; Gnanou, Y. *J. Am. Chem. Soc.* **2000**, *122*, 5929.
(17) Xu, L.; Li, C.; Simon Ng, K. Y. S. *J. Phys. Chem. A* **2000**, *104*, 3952.
(18) Decker, C.; Moussa, K. *Macromolecules* **1989**, *22*, 4455.
(19) Anseth, K. S.; Decker, C.; Bowman, C. N. *Macromolecules* **1995**, *28*, 4040.
(20) Berchtold, K. A.; Lovestead, T. M.; Bowman, C. N. *Macromolecules* **2002**, *35*, 7968.
(21) Pasquale, A. J.; Long, T. E. *Macromolecules* **1999**, *32*, 7954.
(22) Storey, R. F.; Donnalley, A. B.; Maggio, T. L. *Macromolecules* **1998**, *31*, 1523.
(23) Reshadat, R.; Balke, S. T. *Appl. Spectrosc.* **1999**, *53*, 1309.
(24) Lee, D. C.; Ford, J. R.; Fytas, G.; Chu, B.; Hagnauer, G. L. *Macromolecules* **1986**, *19*, 1586.
(25) Liu, T.; Schuch, H.; Gerst, M.; Chu, B. *Macromolecules* **1999**, *32*, 6031.
(26) Florenzano, F. H.; Strelitzki, R.; Reed, W. F. *Macromolecules* **1998**, *31*, 7226.
(27) Reed, W. F. *Macromolecules* **2000**, *33*, 7165.
(28) Drenski, M. F.; Reed, W. F. *Polym. Mater. Sci. Eng.* **2003**, *305*.
(29) Chu, B.; Lee, D. C. *Macromolecules* **1984**, *17*, 926.
(30) Berry, G. C. *Adv. Polym. Sci.* **1994**, *114*, 233.
(31) Hansen, J. P.; McDonald, I. R. *The Theory of Simple Liquids*; Academic Press: New York, 1986.
(32) Nakamura, Y.; Norisuye, T.; Teramoto, A. *J. Polym. Sci., Part B: Polym. Phys.* **1991**, *29*, 153.
(33) Kniewske, R.; Kulicke, W. M. *Makromol. Chem.* **1983**, *184*, 2173.
(34) Appelt, B.; Meyerhoff, G. *Macromolecules* **1980**, *13*, 657.
(35) Bruns, W. *Macromolecules* **1997**, *30*, 4429.
(36) Stockmayer, W. H.; Casassa, E. F. *J. Chem. Phys.* **1952**, *20*, 1560.
(37) Freed, K. H. In *Renormalization Group Theory of Macromolecule;* John Wiley & Sons: New York, 1987.
(38) Sorci, G. A.; Reed, W. F. *Macromolecules* **2002**, *35*, 5218.
(39) Muthukumar, M. *J. Chem. Phys.* **1986**, *85*, 4722.
(40) Casassa, E. F.; Berry, G. C. In *Comprehensive Polymer Science*; Allen, G., Ed.; Pergamon: New York, 1988; Vol. 2.
(41) Yamakawa, H. *Modern Theory of Polymer Solutions*, Harper & Row: New York, 1971.
(42) Dotson, N. A.; Galvan, R.; Laurence, R. L.; Tirrel, M. *Polymerization Process Modeling*; VCH Pub.: New York, 1996; Chapter 3.
(43) Giz, A.; Giz, H.; Brousseau, J. L.; Alb, A.; Reed, W. F. *Macromolecules* **2001**, *34*, 1180.
(44) Tobolsky, A. V. *J. Am. Chem. Soc.* **1958**, *80*, 5927.
(45) Tobolsky, A. V.; Gobran, R. H.; Boehme, R.; Schaffhauser, R. *J. Am. Chem. Soc.* **1963**, *67*, 2336.
(46) Wooster, C. B. *Macromolecules* **1968**, *1*, 324.
(47) Sorci, G. A.; Reed, W. F. *Langmuir* **2002**, *18*, 353.

MA035835J